Sensors and Actuators B 150 (2010) 667–672

Contents lists available at ScienceDirect

Sensors and Actuators B: Chemical

journal homepage: www.elsevier.com/locate/snb

Direct visualization of molecular scale chemical adsorptions on solids using plasmonic nanoparticle arrays

Chaoming Wang[a,b], Liyuan Ma[a], Mainul Hossain[a,c], Haining Wang[d], Shengli Zou[d], James J. Hickman[a,c,d], Ming Su[a,b,*]

[a] NanoScience Technology Center, University of Central Florida, Orlando, FL 32826, United States
[b] Department of Mechanical, Materials, and Aerospace Engineering, University of Central Florida, Orlando, FL 32826, United States
[c] School of Electrical Engineering and Computer Science, University of Central Florida, Orlando, FL 32826, United States
[d] Department of Chemistry, University of Central Florida, Orlando, FL 32826, United States

ARTICLE INFO

Article history:
Received 26 April 2010
Received in revised form 14 August 2010
Accepted 18 August 2010
Available online 26 August 2010

Keywords:
Plasmonic nanoparticles
Visual detection
Adsorption
Molecular thin film
Mercury

ABSTRACT

The fast and sensitive detections of chemicals adsorption onto solid substrates are of importance to many fields. Ordered arrays of gold or silver nanoparticles with strong surface plasmon resonances allow directly visualized detections of molecular scale adsorptions of polymer multilayers, an explosive derivative, and mercury vapor on solid substrates. The adsorbed species change local dielectric constants surrounding plasmonic nanoparticles, leading to shifts of plasmon resonance peaks into either long or short wavelength direction depending on interactions of chemicals with nanoparticles. The magnitude of peak shifts is proportional to the amount of adsorbed chemicals in certain range, and is sufficiently large so that color changes can be seen directly by naked eyes. The ordered nanoparticles can be made over a large area at high yield, allowing a quantitative, passive, and sensitive detection of molecular species.

1. Introduction

The ability to detect and monitor chemicals adsorbed on solid substrates with high precision and low cost is important for many industrial fields such as fabrications of thin films for optical or electronic devices, reductions of friction or wear using lubricant films and constructions of bio-compatible or bio-repelling surface films. A variety of techniques have been used to detect adsorbed species using optical or conductometric sensors, quartz crystal microbalance and cantilever [1–8]. The advent of nanostructured materials has created many opportunities to dramatically enhance the ability to detect adsorbed chemicals. Nanoparticles with unique optical, magnetic, electronic, and chemical properties have been used either alone or as functional additives to improve performance of molecular detections, where changes in the physical properties of nanoparticles reflect existences or concentrations of target molecules [9–19]. Due to small size and large surface area to volume ratio of the nanoparticles, the detection sensitivity is enhanced and response time is shortened [20–22]. In particular, nanoparticles of noble metals including gold and silver have shown strong surface plasmonic effects. Once these nanoparticles are assembled to form an ordered array onto a dielectric substrate, an incoming white light can excite the surface plasmons, which coherently resonate with those of nearby nanoparticles, causing extinction or scattering of light with improved efficiency. The surface plasmon resonance (SPR) peak shifts upon adsorption of molecules due to changes in dielectric constant of local medium, and provides a means of signal transduction [23–26]. The structure, composition, surface properties, and the assembly of nanoparticles can be precisely tuned to allow bottom–up constructions of nanostructured materials with controlled properties [27–31]. But, plasmonic sensors rely on optical spectrometers to detect shifts of plasmon resonance peak. A particular area of interest is the detection of mercury vapor, which can affect the lungs, kidneys, skin, eyes, and nervous and immune systems of human. As mercury containing products (i.e., fluorescent lighting) and industrial processes (i.e., coal burning power generation and solid waste incinerations) become more and more popular, there is the need to conveniently detect mercury vapor in air over a large area [32,33].

We report the detection of low concentration molecules including polymer, mercury vapor, and an explosive derivative, 2,4-dinitrotoluene (DNT), by directly visualizing color changes of an ordered array of plasmon nanoparticles deposited on glass substrates (Fig. 1). The adsorption of molecules onto

* Corresponding author at: NanoScience Technology Center, University of Central Florida, 12424 Research Parkway, Suite 400, Orlando, FL 32826, United States. Tel.: +1 407 882 2822; fax: +1 407 882 2819.
E-mail address: mingsu@mail.ucf.edu (M. Su).

0925-4005/$ – see front matter © 2010 Elsevier B.V. All rights reserved.
doi:10.1016/j.snb.2010.08.022

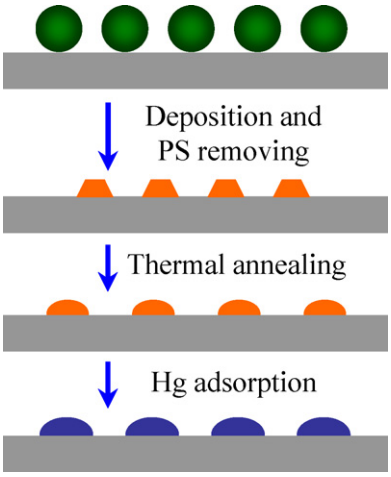

Fig. 1. Schematic illustration of color change of gold nanoparticles upon deposition of different molecular thin films (mercury, DNT and polyelectrolyte multilayers).

metal nanoparticles changes local dielectric constants, and optical appearance of glass substrates. In case of mercury vapor, chronic exposure to mercury is monitored by detecting accumulated color changes of gold nanoparticles that have high affinity with mercury. The amalgamated nanoparticles can be regenerated by heating the substrate up to a high temperature (300 °C), providing a passive, low cost, and convenient way to detect mercury vapor. Gold nanoparticles can be deposited onto a large substrate to allow solid state capture of mercury, which enables simultaneous mercury sensing and capturing. In case of explosive detection, the explosive vapor condenses on solid surface, changes local dielectric constant and leads to color change of the substrate. In addition, polymer multilayers that have precisely controlled thicknesses have been used as a standard to reflect or calibrate the detection capability of this method.

2. Experiments

2.1. Chemicals

All the chemicals used in this experiment are reagent grade and used without further purification. Borosilicate glass microscope slides are obtained from VWR (West Chester, PA). The glass slides are thoroughly cleaned by H_2SO_4, NH_4OH and H_2O_2 at certain concentration following standard procedures. Surfactant-free carboxyl-modified polystyrene suspension containing 4% of solid nanospheres (diameter 400 nm) is obtained from Invitrogen (Carlsbad, CA). Ultrapure water with resistivity of 18.2 MΩ cm^{-1} is obtained from a Millipore system (Marlborough, MA), and used to clean glass and make solutions. High purity gold, silver and chromium are obtained from Goodfellow (Oakdale, PA) as source materials for thermal or electron beam evaporations. Poly(acrylic acid) (PAA) with molecular weight of 90,000 and poly(alkylamine hydrochloride) (PAH) with molecular weight of 70,000 are obtained from Polysciences and Aldrich, respectively. Mercury and 2,4-dinitrotoluene (DNT) are used by delivering their vapor into a detection chamber using continuous flow of nitrogen.

2.2. Template preparation

Glass microscope slides are cut into small regular pieces and cleaned at 80 °C for 30 min in a piranha solution that contains 3:1 concentrated H_2SO_4:30% H_2O_2, and rinsed repeatedly using deionized water (resistivity 18.2 MΩ cm^{-1}) until the pH value of the solution reaches 6. This cleaning removes organic contaminants from slides. The slides are then sonicated in 5:1:1 H_2O:NH_4OH:H_2O_2 solution for 60 min, and washed with large amount of water until pH value reaches 6 again. After such treatment, the slides become very hydrophilic due to the production of hydroxyl groups. The prepared slides are stored in deionized water and used within one week. In order to form nanosphere mask, ~2.5 μl of nanosphere solution at original concentration is dropped onto a cleaned glass slide that has a thin water film. The existence of such film can facilitate the diffusion of nanospheres over the glass substrate and prevent the fast drying of suspension. Then the slide is stored inside a covered Petri dish to allow the slow evaporation of water, which is helpful to form a closely packed monolayer of nanospheres.

2.3. Preparation of periodic silver/gold nanoparticle arrays

The ordered nanoparticle arrays are produced on glass substrates using nanosphere lithography and thermal evaporation of metallic films (Fig. 1) [34]. Briefly, 2 nm of chromium and 40 nm of silver (or gold) are evaporated onto glass substrates through interstitial spaces of densely packed monolayer of polystyrene (PS) nanospheres. The thicknesses of films are monitored using quartz crystal microbalance. After taking samples out of the evaporator, the nanospheres are removed by sonicating samples in absolute ethanol for 3 min. An atomic force microscope (AFM) operated in tapping mode is used to image nanoparticles. AFM image shows that triangular-shaped silver (or gold) nanoparticles are arranged to form ordered hexagonal patterns. After annealing the samples, coated with gold nanoparticles, at 600 °C for 10 h in air, the triangular nanoparticles have transformed into hemispheric nanoparticles. The diameter and interparticle spacing of nanoparticles are determined by the diameters of nanospheres and are 50 and 230 nm, respectively. The height of annealed nanoparticles is determined by AFM as 20 nm. X-ray diffraction (XRD) spectrum shows annealed gold nanoparticles are well-crystallized with strong diffraction peaks [35]. All AFM images presented here are unfiltered draw data.

2.4. Polyelectrolyte multilayer films

Polyelectrolyte multilayers are deposited on the silver (or gold) nanoparticle arrays through layer-by-layer method. The multilayers are deposited from 0.01 M solutions of PAA and PAH at pH of 3.5 and 8.5, respectively. The deposition involves the immersion of charged surfaces (i.e., glass) into the aqueous solutions of both polyanions and polycations in an alternating sequence to built multilayers by electrostatic interaction. Briefly, the glass slides are immersed in the PAH solution for 15 min, and rinsed with DI water for three times in separate beakers. The slides are then immersed in the PAA solution for 15 min and rinsed with DI water for three times as well. Such deposition cycle is repeated for n times to deposit n bilayers of PAH and PAA.

2.5. Ultraviolet–visible extinction spectroscopy

The glass slides with nanoparticles are placed in a self-built detection cell, which has an inlet and an outlet to allow liquid or gas to pass continuously. The two sides of the cell are transparent. UV–vis extinction measurements are performed using a fiber optical mini-spectrophotometer (Ocean Optics, FL) with charge coupled device (CCD) detector. The multimode fiber permits the passage of light in the wavelength region from 400 to 900 nm. All spectra are collected in transmission mode using normally incident, non-polarized white light with beam size of about 2 mm^2. Each spectrum is an average of 25 individual ones at 8 ms integrations, and the collection is performed in either dry nitrogen or deionized water.

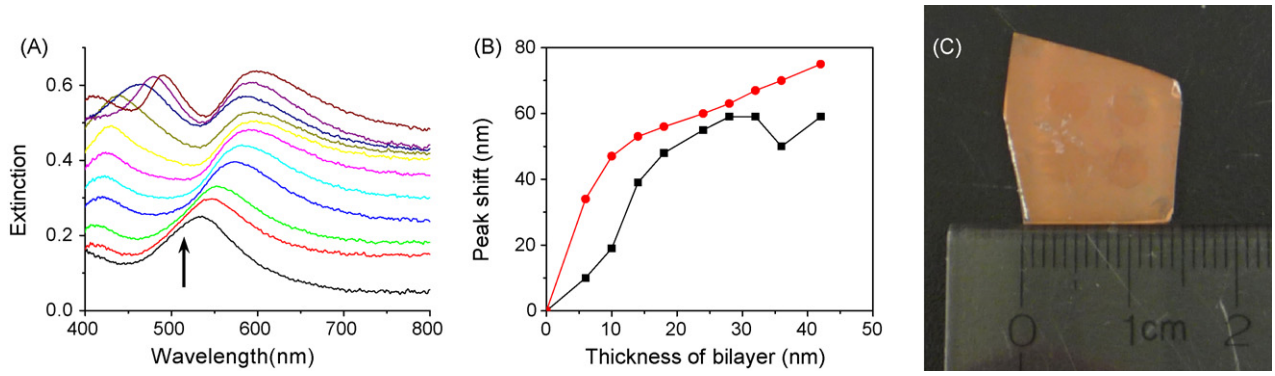

Fig. 2. (A) The UV–visible extinction spectra of silver nanoparticle array with 0–10 bilayers of PAH/PAA (bottom to up), respectively; (B) the experimental (square) and simulated (circle) peak shifts as functions of numbers of bilayers, respectively; (C) a micrograph of circle patterns that have been covered by three bilayers of PAH/PAA.

2.6. Discrete dipole approximation

The plasmonic resonance peak shift is modeled using a finite element electrodynamics method known as the discrete dipole approximation (DDA). Both the nanoparticle and surrounding multilayer dielectric are represented in terms of cubical elements, and the optical response to an applied plane wave field is used to calculate extinction cross-sections.

3. Results and discussion

UV–vis extinction spectra of silver (or gold) nanoparticles are collected after depositing polyelectrolyte multilayers. Fig. 2A shows the extinction spectra of an ordered silver nanoparticles array in dried nitrogen after depositing 1–10 multilayers, where the resonance peak does not shift after 7 multilayers, suggesting saturation of plasmonic signal. The new peaks appear at about 470 nm can be assigned to quadrupole oscillations. Fig. 2B shows the plotted shifts of resonance peaks versus the number of bilayers, where a linear dependence of peak shifts on the number of bilayers can be seen before reaching saturated values. More interestingly, the color change of gold nanoparticles can be observed by making micropatterns on the substrate (Fig. 2C), which allows to conveniently monitor polymer multilayers. Similarly, thin films of 2,4-dinitrotoluene (DNT) (melting temperature of 71 °C), which is a derivative of an explosive 2,4,6-trinitrotoluene (TNT), are thermally deposited onto an annealed nanoparticle arrays. The thickness is controlled by exposing nanoparticles to vapor for different time (from 5 to 25 s), and measured using AFM. The deposited films change local dielectric constant around each nanoparticle, and lead to shifts of plasmon resonance peaks (Fig. 3A). The deposited DNT thin films can also change color of the gold nanoparticle arrays (Fig. 3B), suggesting that the color change could be a general phenomenon of plasmon nanoparticle arrays.

The polymer multilayer offers a system to investigate the structural dependent optical property of silver nanoparticles. According to the Mie theory and an empirical relation, the peak shift can be related to the thickness of PAH/PAA thin films using [36,37]:

$$\Delta\lambda_{\max} = m(n_{\text{polymer}} - n_{\text{medium}})\left[1 - \exp\left(-\frac{Nt}{l_d}\right)\right]$$

where m is the plasmon excitation coefficient of metal, N is the number of polymer bilayers, n_{polymer} and n_{medium} are the refractive indexes of polymer and medium, respectively, t is the thickness of each layer, and l_d is the characteristic decay length of electromagnetic field surrounding nanoparticle. The equation shows as N increases, $\Delta\lambda$ increases initially. After depositing a certain number of layers, the exponential term becomes dominant, and $\Delta\lambda$ ceases to increase. The plasmon excitation coefficient (m) of silver is taken as 191 [38]. The bulk refractive indexes of polymer and air (nitrogen) are taken as 1.51 and 1.0, respectively. Fig. 2B shows simulated wavelength shift at different thickness (red), where the characteristic decay length of electromagnetic field is derived to be 30 nm with the average thickness on PAH/PAA bilayer of 5 nm [39], and a 10 nm thick polymer film leads to 25 nm wavelength shifts of plasmon peak in nitrogen in the linear region of the curve. (For interpretation of the references to color in this figure, the reader is referred to the web version of the article.).

A glass substrate with gold nanoparticles is installed inside a self-built chamber that has an inlet and outlet to allow mercury vapor to be delivered by nitrogen flow. The concentration of mercury vapor is determined by vapor pressure of mercury at room

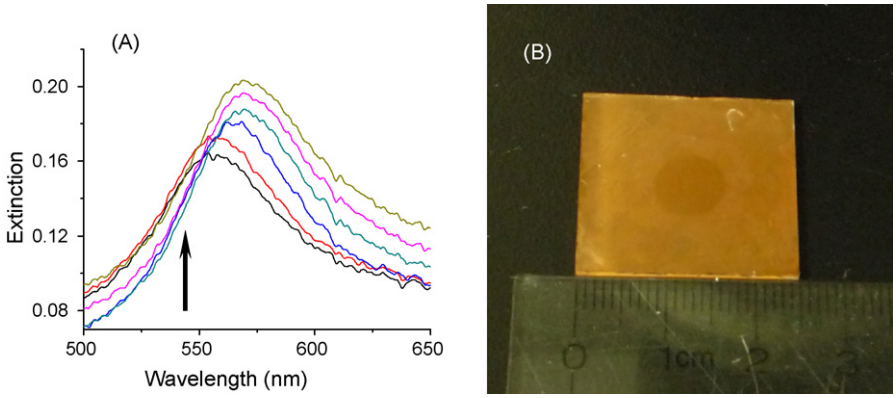

Fig. 3. (A) The extinction spectra of gold nanoparticles after exposing to DNT vapor, where the curves are taken at 0, 5, 10, 15, 20 and 25 s (bottom to up), respectively; (B) a micrograph of a circle pattern not exposed to DNT.

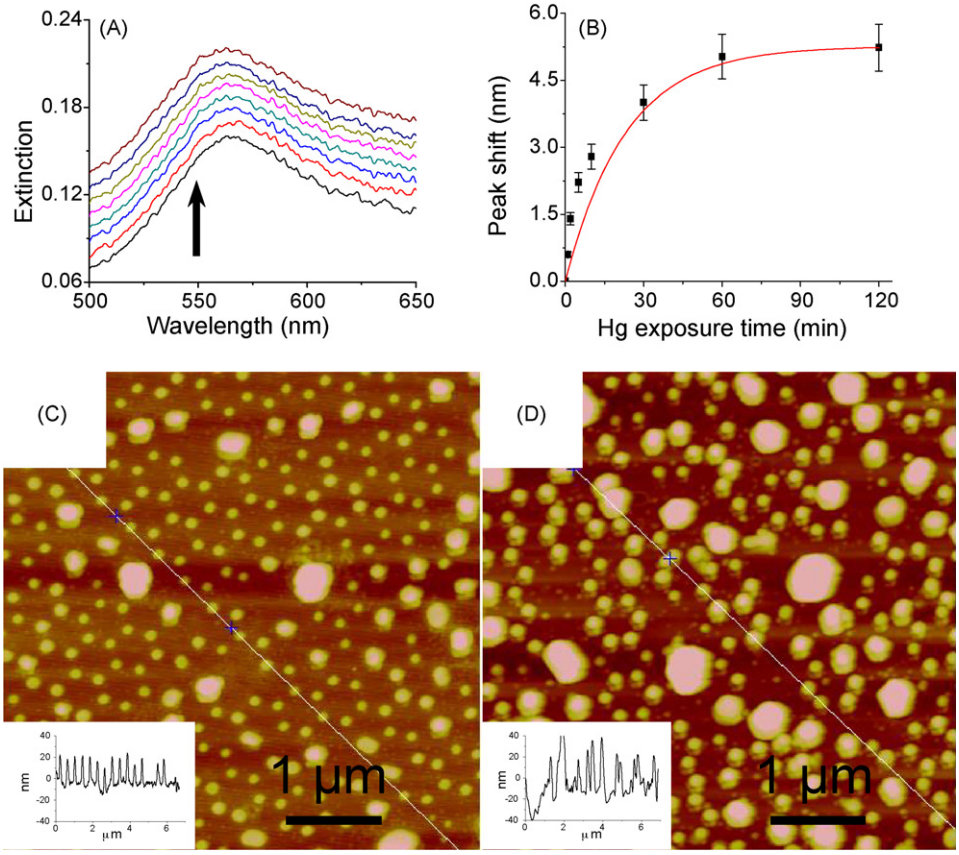

Fig. 4. The peak shifts of gold nanoparticles after exposed to 15 ppm mercury vapor (A), where the curves are taken at 0, 1, 2, 5, 10, 30, 60 and 120 min (bottom to up), respectively; (B) the magnitude of peak shifts at different exposure time; AFM images of nanoparticles before (C) and after (D) exposing to mercury for 120 min, where insets show the according cross-section profiles.

temperature and flow rate of nitrogen. Fig. 4A shows the peak shifts when gold nanoparticles are exposed to 15 ppm of mercury vapor for certain time, where each curve is vertically shifted for display purpose. The peak shifts towards short wavelength direction from 565 to 560 nm and saturates after about 2 h' exposure. The magnitude of peak shift is plotted as the function of exposure time (Fig. 4B), where a monotonic peak shifts can be seen. The response rate on gold nanoparticles to mercury vapor has been compared to that on gold thin film. At exposure time of 30 min, the magnitude of peak shift (4.25 nm) is 85% of the total peak shift (5 nm), which is faster than 67% collected on thin film [40]. The fast response is attributed to large surface area to volume ratio of nanoparticles. The nanoparticles can also be regenerated by heating the mercury exposed sample to remove mercury: when temperature is kept at 300 °C for 30 min, the plasmon resonance peak shifts to long wavelength and return to original values. The regeneration can be done for few times without deteriorating the sensing behaviors.

In order to confirm the origin of peak shifts, the gold nanoparticles before and after exposing to mercury vapor are imaged by AFM. Fig. 4C and D show AFM images of gold nanoparticles before and after exposing to 15 ppm of mercury vapor for 2 h, respectively. Nanoparticles after exposure (Fig. 4D) are larger than those in Fig. 4C at the same magnification. From the cross-section profiles of images (Fig. 4C and D, insets), the height of nanoparticles after mercury exposure is derived to be 30 nm, which is taller than before exposure (20 nm). Although the lateral dimension derived from AFM does not reflect actual value because of the broadening effect of AFM imaging, the heights of nanoparticles can be reflected accurately. If the ratio of expansion is identical in each direction, the volume increase of a hemispheric nanoparticle with height of 30 nm is 3.4 times as that of a 20 nm hemispheric nanoparticle. Taking densities of gold (19.3 g/ml) and mercury (13.5 g/ml), the gold to mercury mass ratio is derived to be 0.6. The adsorption of mercury increases the volume of gold nanoparticles, and changes the effective refraction index, which leads to blue shift of SPR peaks. Although the peak shifts is relatively small (5 nm), the color change of gold nanoparticles upon mercury exposure can be visualized by naked eyes or using optical microscope. We have made micropatterns on a glass substrate that has an ordered array of gold nanoparticles. After forming a thin film of photoresist, the glass substrate is radiated with UV light (254 nm) through a mask. After developing the UV radiated area, the sample is exposed to 15 ppm mercury vapor for 16 h. Then the photoresist is removed, and the sample is checked by an optical microscope. Fig. 5A shows the optical contrasts between mercury exposed areas and those of unexposed areas, where the bright regions have not been exposed to mercury vapor. Reversing contrast in photomask makes micropatterns with reversed contrast (Fig. 5B). Energy dispersive X-ray (EDX) spectroscopy shows that the circle contains gold and mercury (Fig. 5C). If the pattern is large enough, the optical contrast can be seen by naked eyes (Fig. 5D).

The blue shift of plasmon peak upon adsorption of metal vapor is general. Indium powder is heated to 600 °C and carried into the detection chamber by nitrogen flow. Upon exposure to indium vapor, the plasmon peak of gold nanoparticles shifts to short wavelength (Supporting Fig. A). Silver nanoparticles deposited on glass surfaces have been exposed to mercury vapor to confirm the blue shift, where the peak shifts to short wavelength as well (Supporting Fig. B). Since mercury has higher vapor pressure than most of met-

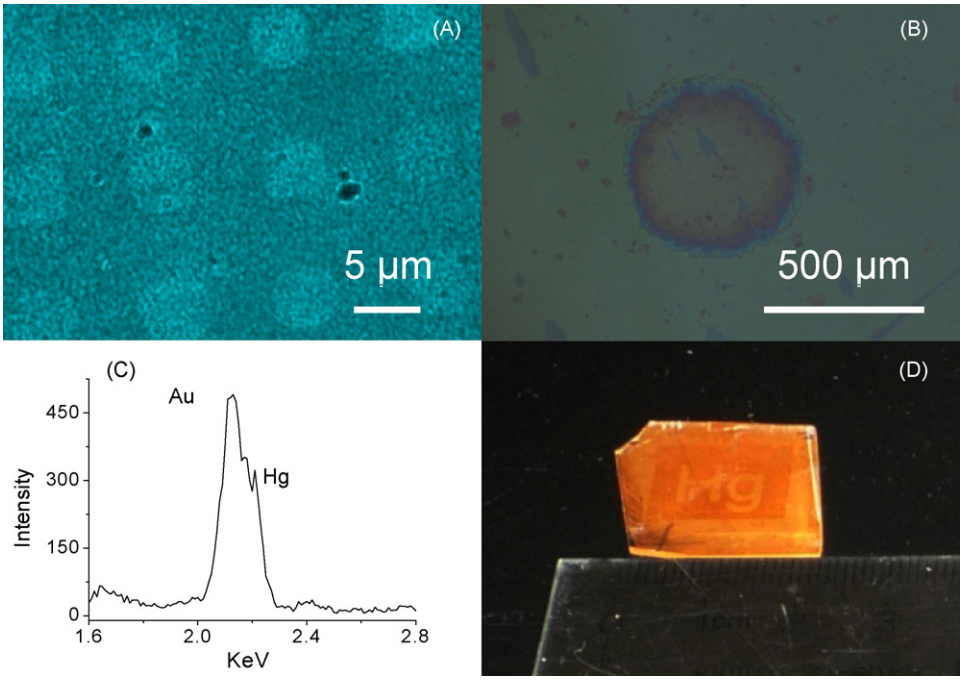

Fig. 5. An optical micrograph of micropatterns produced in mercury vapor on a patterned substrate with gold nanoparticles (A), where the relative white areas are not exposed to mercury vapor; a micropattern produced on a glass substrate with gold nanoparticles in mercury vapor (B), where circle area is exposed to mercury vapor; an EDX spectrum collected from a circle micropattern (B) after exposing to mercury vapor (C); a graph of a character produced after exposing to mercury vapor on a 2 cm × 2 cm glass with an ordered array of gold nanoparticles (D).

als, the method of mercury detection using gold nanoparticles has high specificity. Furthermore, gold nanoparticles can be deposited on a large glass surface to capture an appreciable amount of mercury while monitoring mercury concentration. We have made a large array of gold nanoparticles on a 7.5 cm × 7.5 cm glass substrate (Supporting Fig. C), which can be used as a window material to monitor and capture mercury vapor in air. If the nanoparticles contain 40% (mass ratio) of mercury, the mass of mercury that can be taken by nanoparticles on this glass is over 0.05 mg without affecting appearance of glass. Such number can reach 80 mg if surface area is increased to 10 m^2. Providing that good circulation of air is maintained, 80 mg of mercury vapor floating in air can be captured on a 10 m^2 glass in 1 h.

4. Conclusions

In conclusion, the molecular adsorptions on solid substrates can be sensitively and conveniently detected by shifts of surface plasmon resonance peaks. The peak shifts in cases of polymer film, mercury vapor, and DNT are sufficiently large in certain range that color changes can be directly visualized by naked eyes. Gold nanoparticles can be regenerated after mercury adsorption, and can be produced over a large area to capture mercury in air. Compared to existing techniques of detecting chemical adsorption, this method involving plasmonic nanoparticles can be widely deployed to detect chemicals over a large area in a fast and convenient way. Meanwhile, structural engineering of nanoparticle array can further enhance the detection sensitivity.

Acknowledgements

This work has been supported by the Florida Department of Health, National Science Foundations (CBET), ACS Petroleum research fund (ACS/PRF), Office of Naval Research (ONR), and University of Central Florida (UCF). Some characterizations are done at the Materials Characterization Facilities (MCF) of UCF. C. Wang and L. Ma have equal contribution to this work.

Appendix A. Supplementary data

Supplementary data associated with this article can be found, in the online version, at doi:10.1016/j.snb.2010.08.022.

References

[1] M.A. Butler, A.J. Ricco, R.J. Baughman, Hg adsorption on optically thin Au films, J. Appl. Phys. 67 (1990) 4320–4326.
[2] R.W. Fane, W.E.J. Neal, R.M. Rollason, Detection of oil or mercury on surfaces in vacuum systems using an ellipsometer, Appl. Phys. Lett. 12 (1968) 265–266.
[3] O.I. Matveev, B.W. Smith, J.D. Winefordner, A low pressure mercury vapor resonance ionization image detector, Appl. Phys. Lett. 72 (1998) 1673–1675.
[4] B. Mazzolai, V. Mattoli, V. Raffa, G. Tripoli, D. Accoto, A. Menciassi, P. Dario, A microfabricated physical sensor for atmospheric mercury monitoring, Sens. Actuators A 113 (2004) 282–287.
[5] J.J. McNerney, P.R. Buseck, C.H. Roland, Mercury detection by means of thin gold films, Science 178 (1972) 611–612.
[6] M.G. Schweyer, J.C. Andle, D.J. McAllister, J.F. Vetelino, An acoustic plate mode sensor for aqueous mercury, Sens. Actuators B 35 (1996) 170–175.
[7] T. Thundat, E.A. Wachter, S.L. Sharp, R.J. Warmack, Detection of mercury-vapor using resonating microcantilevers, Appl. Phys. Lett. 66 (1995) 1695–1697.
[8] X.J. Xue, F. Wang, X.G. Liu, One-step, room temperature, colorimetric detection of mercury (Hg^{2+}) using DNA/nanoparticle conjugates, J. Am. Chem. Soc. 130 (2008) 3244–3245.
[9] F. Caruso, K. Niikura, D.N. Furlong, Y. Okahata, Assembly of alternating polyelectrolyte and protein multilayer films for immunosensing, Langmuir 13 (1997) 3427–3433.
[10] G. Kalyuzhny, M.A. Schneeweiss, A. Schanzer, A. Vaskevich, I. Rubinstein, Different plasmon spectroscopy as a tool for monitoring molecular binding to ultrathin gold films, J. Am. Chem. Soc. 123 (2001) 3177–3178.
[11] J.J. Lai, J.M. Hoffman, M. Ebara, A.S. Hoffman, C. Estournes, A. Wattiaux, P.S. Stayton, Dual magnetic-/temperature-responsive nanoparticles for microfluidic separations and assays, Langmuir 23 (2007) 7385–7391.
[12] D. Li, A. Wieckowska, I. Willner, Optical analysis of Hg^{2+} ions by oligonucleotide–gold-nanoparticle hybrids and DNA-based machines, Angew. Chem. Int. Ed. 47 (2008) 3927–3931.
[13] N. Nath, A. Chilkoti, A colorimetric gold nanoparticle sensor to interrogate biomolecular interactions in real time on a surface, Anal. Chem. 74 (2002) 504–509.
[14] R. Pohle, M. Fleischer, H. Meixner, In situ infrared emission spectroscopic study of the adsorption of H_2O and hydrogen-containing gases on Ga_2O_3 gas sensors, Sens. Actuators B 68 (2000) 151–156.
[15] J.C. Riboh, A.J. Haes, A.D. Mcfarland, C.R. Yonzon, R.P. Van Duyne, A nanoscale optical biosensor: real-time immunoassay in physiological buffer

enabled by improved nanoparticle adhesion, J. Phys. Chem. B 107 (2003) 1772–1780.
[16] T. Selvaraju, J. Das, K. Jo, K. Kwon, C.-H. Huh, T.K. Kim, H. Yang, Nanocatalyst-based assay using DNA-conjugated Au nanoparticles for electrochemical DNA detection, Langmuir 24 (2008) 9883–9888.
[17] Y.G. Sun, Y.N. Xia, Increased sensitivity of surface plasmon resonance of gold nanoshells compared to that of gold solid colloids in response to environmental changes, Anal. Chem. 74 (2002) 5297–5305.
[18] S. Tan, M. Erol, S. Sukhishvili, H. Du, Substrates with discretely immobilized silver nanoparticles for ultrasensitive detection of anions in water using surface-enhanced Raman scattering, Langmuir 24 (2008) 4765–4771.
[19] J. Yang, K. Eom, E.-K. Lim, J. Park, Y. Kang, D.S. Yoon, S. Na, E.K. Koh, J.-S. Suh, Y.-M. Huh, T.Y. Kwon, S. Haam, In situ detection of live cancer cells by using bioprobes based on Au nanoparticles, Langmuir 24 (2008) 12112–12115.
[20] Y.W. Charles, R.C. Jin, C.A. Mirkin, Nanoparticles with Raman spectroscopic fingerprints for DNA and RNA detection, Science 297 (2002) 1536–1540.
[21] M.A. Roberts, S.O. Kelley, Ultrasensitive detection of enzymatic activity with nanowire electrodes, J. Am. Chem. Soc. 129 (2007) 11356–11357.
[22] G.F. Zheng, F. Patolsky, Y. Cui, W.U. Wang, C.M. Lieber, Multiplexed electrical detection of cancer markers with nanowire sensor arrays, Nat. Biotechnol. 23 (2005) 1294–1301.
[23] A.J. Haes, R.P. Van Duyne, A nanoscale optical biosensor: sensitivity and selectivity of an approach based on the localized surface plasmon resonance spectroscopy of triangular silver nanoparticles, J. Am. Chem. Soc. 124 (2002) 10596–10604.
[24] M.D. Malinsky, K.L. Kelly, G.C. Schatz, R.P. Van Duyne, Chain length dependence and sensing capabilities of the localized surface plasmon resonance of silver nanoparticles chemically modified with alkanetiol self-assembled monolayers, J. Am. Chem. Soc. 123 (2001) 1471–1482.
[25] T. Morris, H. Copeland, E. McLinden, S. Wilson, G. Szulczewski, The effects of mercury adsorption on the optical response of size-selected gold and silver nanoparticles, Langmuir 18 (2002) 7261–7264.
[26] D. Yang, H.-H. Lu, B. Chen, C.-W. Lin, Surface plasmon resonance of SnO2/Au bilayer films for gas sensing applications, Sens. Actuators B 145 (2010) 832–838.
[27] M.A. Elsayed, Some interesting properties of metals confined in time and nanometer space of different shapes, Acc. Chem. Res. 34 (2001) 257–264.
[28] X.-J. Huang, Y.-K. Choi, Chemical sensors based on nanostructured materials, Sens. Actuators B 122 (2007) 659–671.
[29] E. Hutter, J.H. Fenddler, Exploitation of localized surface plasmon resonance, Adv. Mater. 16 (2004) 1685–1706.
[30] M.G. Manera, P. Davide Cozzoli, G. Leo, M. Lucia Curri, A. Agostiano, L. Vasanelli, R. Rella, Thin films of TiO_2 nanocrystals with controlled shape and surface coating for surface plasmon resonance alcohol vapour sensing, Sens. Actuators B 126 (2007) 562–572.
[31] S. Underwood, P. Mulvaney, Effect of the solution refractive index on the color of gold colloids, Langmuir 10 (1994) 3427–3430.
[32] Y. Liu, D.J.A. Kelly, H. Yang, C.C.H. Lin, S.M. Kuznicki, Z. Xu, Novel regenerable sorbent for mercury capture from flue gases of coal-fired power plant, Environ. Sci. Technol. 42 (2008) 6205–6210.
[33] F.M.M. Morel, A.M.L. Kraepiel, M. Amyot, The chemical cycle and bioaccumulation of mercury, Annu. Rev. Ecol. Syst. 29 (1998) 543–566.
[34] J.C. Hulteen, D.A. Treichel, M.T. Smith, M.L. Duval, T.R. Jensen, R.P. Van Duyne, Nanosphere lithography: size-tunable silver nanoparticle and surface cluster arrays, J. Phys. Chem. B 103 (1999) 3854–3863.
[35] C. Wang, M. Zhang, H. Wang, S. Zou, M. Su, Subnanogram mass measurements on plasmonic nanoparticles for temperature-programmed thermal analysis, J. Phys. Chem. Lett. 1 (2010) 79–84.
[36] C.L. Haynes, R.P. Van Duyne, Nanosphere lithography: a versatile nanofabrication tool for studies of size-dependent nanoparticle optics, J. Phys. Chem. B 105 (2001) 5599–5611.
[37] G. Mie, Contributions to the optics of turbid media, especially colloidal metal solutions, Ann. Phys. 25 (1908) 377–445.
[38] D.E. Charles, D. Aherne, M. Gara, D.M. Ledwith, Y.K. Gunko, J.M. Kelly, W.J. Blau, M.E. Brennan-Fournet, Versatile solution phase triangular silver nanoplates for highly sensitive plasmon resonance sensing, ACS Nano 4 (2010) 55–64.
[39] S.S. Shiratori, M.F. Rubner, pH-dependent thickness behavior of sequentially adsorbed layers of weak polyelectrolytes, Macromolecules 33 (2000) 4213–4219.
[40] T. Morris, G. Szulczewski, A spectroscopic ellipsometry, surface plasmon resonance, and X-ray photoelectron spectroscopy study of Hg adsorption on gold surfaces, Langmuir 18 (2002) 2260–2264.

Biographies

Chaoming Wang is a PhD. student in the NanoScience Technology Center and the Department of Mechanical, Materials, and Aerospace Engineering at the University of Central Florida. His research interest is on nanoparticles for sensing applications.

Liyuan Ma is a research assistant professor at the NanoScience Technology Center at the University of Central Florida. Her research interest is on nanoparticle biosensing, and nanostructure-enhanced mass spectrometry for cancer research.

Mainul Hossain is currently a PhD. student at the NanoScience Technology Center and the School of Electrical Engineering and Computer Science at the University of Central Florida. His research is on nanoparticle enhanced cancer treatment by radiation therapy.

Haining Wang is currently a PhD student at the Department of Chemistry at the University of Central Florida. His research is on the modeling of plasmonic nanostructures.

Shengli Zou is currently an assistant professor at the Department of Chemistry, University of Central Florida. His research interest includes the optical properties of nanoparticles.

James J. Hickman is a professor at the NanoScience Technology Center at the University of Central Florida. His research is focused on neuroscience, microelectronics, and cell biology.

Ming Su is currently an assistant professor in the NanoScience Technology Center and the Department of Mechanical, Materials and Aerospace Engineering at the University of Central Florida. His research includes nanoparticles for biological applications.